IEEE Access
Multidisciplinary | Rapid Review | Open Access Journal

Received May 16, 2021, accepted May 25, 2021, date of publication May 27, 2021, date of current version June 7, 2021.

Digital Object Identifier 10.1109/ACCESS.2021.3084457

A Frequency and Voltage Stability-Based Load Shedding Technique for Low Inertia Power Systems

NAHID-AL-MASOOD[1], (Senior Member, IEEE), MD. NAHID HAQUE SHAZON[1,2], (Student Member, IEEE), SHOHANA RAHMAN DEEBA[3], (Member, IEEE), AND SEEMA RANI MODAK[4]

[1]Department of Electrical and Electronic Engineering, Bangladesh University of Engineering and Technology, Dhaka 1205, Bangladesh
[2]Department of Electrical and Electronic Engineering, BRAC University, Dhaka 1212, Bangladesh
[3]Department of Electrical and Computer Engineering, North South University, Dhaka 1229, Bangladesh
[4]Department of Electrical and Electronic Engineering, Daffodil International University, Dhaka 1207, Bangladesh

Corresponding author: Nahid-Al-Masood (nahid@eee.buet.ac.bd)

ABSTRACT The aim of this research work is to develop a load shedding methodology to improve the frequency response of low inertia grids by attaining satisfactory voltage stability. In recent times, wind energy integration has considerably increased in many power grids. Consequently, conventional synchronous machines are being replaced from dispatch. Unlike traditional synchronous machines, variable speed wind turbine generators usually do not take part in frequency regulation without supplementary control mechanism. During substantial wind penetration, a power system may have a small number of online synchronous machines. As a result, synchronous inertia and governor responsive reserve significantly reduce. Under such situation, a system has to rely on load shedding as a last line of defense to rescue the system frequency following a large contingency. However, the conventional Under-Frequency Load Shedding (UFLS) strategy may lead to larger frequency deviation and higher amount of load cut in certain cases. A new load shedding methodology is presented in this paper to overcome this challenge. Unlike conventional UFLS technique, higher proportion of load shedding is applied to relatively weaker buses in terms of voltage stability in the proposed mechanism. Based on reactive power margin, which is an index to specify voltage stability, a general expression to quantify load shedding is derived. Also, the adaptability of the proposed strategy to various load levels is ensured. Later on, performances of the developed strategy are explored in a low inertia wind dominated test network. Simulations are executed considering various penetration levels of wind power and for two severe contingencies – loss of 550 MW interconnection and loss of 650 MW interconnection. Investigations reveal that the proposed load shedding methodology ensures satisfactory frequency response in all simulation cases. Also, the developed technique yields less frequency deviation and load cut compared to the conventional UFLS mechanism. Therefore, the reported load shedding scheme is found to be more competent to concurrently maintain frequency and voltage stabilities in renewable dominated power systems.

INDEX TERMS Frequency response, load shedding, low inertia grid, voltage stability, reactive power margin.

NOMENCLATURE

Abbreviations

DFIG	Doubly Fed Induction Generator
FSC	Full Scale Converter
WTG	Wind Turbine Generator
UFLS	Under Frequency Load Shedding
UVLS	Under Voltage Load Shedding
PMU	Phasor Measurement Unit
ROCOF	Rate of Change of Frequency

Notations

$\overline{E}$	Generator voltage in a two-bus system
$\overline{V}$	Load voltage in a two-bus system
Z_{line}	Line impedance

The associate editor coordinating the review of this manuscript and approving it for publication was Yang Li.

Z_{load}	Load impedance
ϕ	Impedance angle of the line
θ	Impedance angle of the load
P_R	Real power supplied to the load
Q_R	Reactive power supplied to the load
N	Number of load buses
Q_{mi}	Inverse of reactive power margin of i-th bus
r_i	Reactive margin factor of i-th load bus
L_i	Total load of i-th bus
$LF_{i,n}$	Load shedding factor of i-th bus in the n-th stage
f	System frequency
f_{thn}	Frequency threshold of the n-th stage of UFLS
IR	System inertia
S_j	MVA rating of j-th synchronous generator
H_j	Inertia constant of j-th synchronous generator
N_C	Total number of online synchronous generators

I. INTRODUCTION

Inadequate frequency response following a large contingency is a major concern in renewable dominated power systems [1]. Prolific penetration of renewable resources, especially wind power integration in transmission levels, causes the replacement of conventional fossil-fuel based synchronous generators from the generation mix [2]. Modern wind machines frequently utilize Type-III and Type-IV (Doubly-Fed Induction Generator: DFIG and Full Scale Converter: FSC respectively) wind turbine generators. These are variable speed machines, which are electrically detached from the corresponding host network via power electronics interfaces. As a result, these WTGs are incapable of offering inertial support and governor response without additional control strategy [3]. Therefore, frequency response of a power system is likely to deteriorate under high wind penetration [4].

A proper balance among overall generation and system load is the key factor to preserve the system frequency stability of a power system. Since the governor responsive reserve is relatively small in low inertia grids, in most cases Under Frequency Load Shedding (UFLS) needs to be come into action to cease the frequency decline. However, the conventional UFLS scheme may not be sufficient to arrest the frequency decline, especially subsequent to a large disturbance (e.g. loss of a major generator or interconnection). Such a failure may eventually lead to system wide blackouts, which are evident from some of the past incidents such as blackouts in Sweden, Denmark and Italy back in 2003, blackout in India in 2012, 2015 and blackout in South Australia back in 2016 [5], [6]. Therefore, further research and explorations are still necessary to design an appropriate load shedding scheme, especially for low inertia power systems.

A number of load shedding schemes are illustrated in the literature to date. In [7], a load shedding methodology is developed for islanded microgrids where initial power deficit is estimated using first derivative of system frequency. However, while estimating power deficit, frequency support from active governors and load frequency relief from frequency dependent loads are ignored. In [8], a probabilistic method for automatic load shedding is proposed, which uses average values of yearly load instead of peak values. Further, UFLS techniques are proposed in [9], [10] to cut optimal amount of load using an adaptive method based on mixed-integer linear programming. Nevertheless, these algorithms do not prioritize different load buses before scheduling load shedding amount. Furthermore, an aggregated state estimator is deployed in [11] to integrate real-time UFLS using traditional weighted least square formulation. Also, UFLS algorithms based on load dynamics [12], Monte Carlo simulation method [13] and equivalent inertia constant [14] are developed. It is well documented that prolific wind penetration instigates serious concerns regarding voltage stability [15], [16]. However, in the aforementioned works [7]–[14], voltage stability issue is ignored. Therefore, the performances of these UFLS techniques under high wind penetration may not be satisfactory.

Apart from UFLS, Under-Voltage Load Shedding (UVLS) schemes are also reported in existing literature. Local measurements are used in [17] to develop a centralized UVLS mechanism to mitigate voltage instability. Another UVLS technique is proposed in [18], which effectively applies load shedding to offset the fault-induced delayed voltage recovery. Furthermore, an adaptive UVLS algorithm is proposed in [19] based on reactive power mismatch among various zones in large interconnected systems. However, these papers do not consider the frequency response adequacy while applying load shedding.

Apart from these studies, a centralized adaptive load shedding approach is proposed in [20], where the optimal amount, location and cost of load interruption are considered along with voltage stability criterion. Further, a centralised-adaptive load shedding approach is reported in [21]. In this method voltage and frequency information are simultaneously utilized, which are provided by Phasor Measurement Units (PMUs). This method concurrently prevents voltage and frequency instabilities. Further, a new index is developed relating the derivative of apparent power and the network admittance in [22] to suggest a load shedding scheme. In addition, optimal amount of load shedding is achieved in [23] by setting priority for loads, which is particularly suitable for smart grid applications. Besides, a two-stage adaptive load shedding mechanism based on PMU measurements in reported in [24]. Here, a system frequency response model is developed in the initial stage, while in the forthcoming stage best location for load cut is specified on the basis of voltage stability. In a recent work [25], a continuous UFLS scheme is reported to shed loads, where amount of load shedding is proportional to frequency deviation. Further, a time-series prediction model based on autoregressive integrated moving average is established to determine the load shedding amounts in [26]. Besides, an adaptive load shedding method is designed using a communication link between remote protective relays and a centralized control center in [27] to take into account the changes of load-level,

system inertia and governor response. In addition, a dynamic-adaptive load shedding algorithm is presented in [28] to concurrently handle frequency and voltage vulnerability. This algorithm uses PMUs to take into account the actual contingency size and subsequently selects the appropriate feeders for load shedding.

It can be inferred from the above discussion that significant attempts are made to develop various load shedding schemes. However, the underlying limitations of the existing techniques are as follows.

- Centralized load shedding methods require communication links, where certain delays are associated. This may compromise the performances of the schemes, particularly for large contingencies.
- Measurement based techniques entail widespread deployment of PMUs, which may be unreasonable in many power systems.
- UFLS schemes alone are unable to ensure voltage stability, while UVLS schemes alone cannot guarantee frequency stability.
- A large number of existing techniques in the literature are validated in conventional power systems, where large renewable penetration is not taken into account.

Therefore, adequate performances of these techniques in low inertia grids under high wind penetration are not assured. To meet the above important yet unaddressed research gaps, this paper aspires to achieve the following contributions.

- A load shedding strategy is proposed to improve the frequency stability of low inertia grids by retaining voltage stability. Notably, the proposed method does not require high speed communication infrastructure and widespread deployment of PMUs.
- In the developed method, higher proportion of load shedding is allocated to relatively vulnerable buses for maintaining voltage stability. To this end, reactive power margin is exploited as an indicator to specify bus strength in terms of voltage stability. Furthermore, a general expression to quantify the load shedding amount is formulated.
- The proposed load shedding strategy is applied to a low inertia wind dominated power system that equivalently represents the South Australian grid. The performance of this scheme is investigated under severe contingencies considering different wind penetration scenarios. Afterwards, the proposed method is validated by correlating and comparing it with a conventional load shedding technique.

Note that both frequency and voltage stabilities deteriorate with a rise in wind penetration level. Since the proposed methodology simultaneously considers frequency and voltage stability aspects, it is rational to proclaim that the method would provide satisfactory performance in modern renewable dominated weak power systems. Thus, outcomes of this paper will be helpful for power utilities to enhance frequency resilience by preserving voltage stability under high renewable penetration.

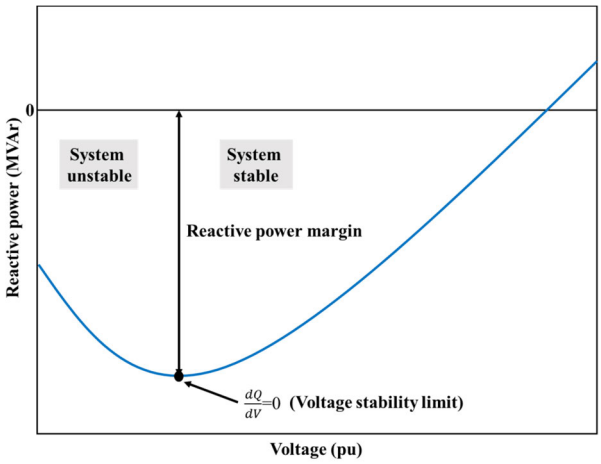

FIGURE 1. An example of a Q-V curve [29].

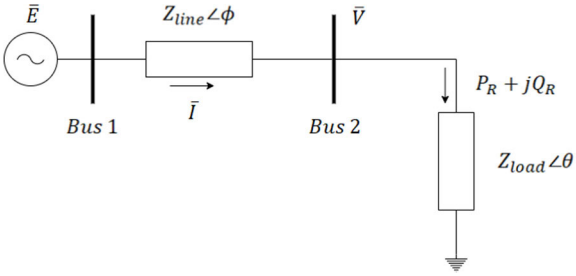

FIGURE 2. A two-bus power system.

II. METHODOLOGY

In this research work, a load shedding methodology is designed to simultaneously retain frequency and voltage stabilities. In this method, reactive power margin is deployed as a tool to determine the required amount of load to be shed at each P-Q bus. UFLS relays are set such that weaker buses encounter relatively higher amount of load cut. For better understanding of the proposed technique, at first reactive power margin is explained below.

A. REACTIVE POWER MARGIN

The reactive power margin of a load (P-Q) bus is defined as the MVAr distance among the nadir point of Q-V curve and voltage axis [29], [30] as shown in Fig. 1. The lowest point of the Q-V curve denotes the voltage collapse point. The lowest reactive power margin manifests that the corresponding bus is the weakest bus in a network. The fundamental concept of constructing a Q-V curve is discussed below.

Let us consider a simple two bus power system illustrated in Fig. 2.

Let $\overline{E}$ and $\overline{V}$ be the generator voltage and load voltage respectively, $\overline{Z}_{line}$ and $\overline{Z}_{load}$ be the line impedance and load impedance respectively, and P_R and Q_R be the real and reactive power supplied to the load respectively. Also, φ and θ

are the impedance angle of line and load respectively. The line current $\bar{I}$ can be expressed using Eq. (1).

$$\bar{I} = \frac{\bar{E}}{\bar{Z}_{line} + \bar{Z}_{load}} \tag{1}$$

Expanding Eq. (1), the magnitude of current can be expressed as,

$$I = \frac{E}{\sqrt{(Z_{line}\cos\phi + Z_{load}\cos\theta)^2 + (Z_{line}\sin\phi + Z_{load}\sin\theta)^2}} \tag{2}$$

Assuming,

$$A = 1 + \left(\frac{Z_{load}}{Z_{line}}\right)^2 + 2\left(\frac{Z_{load}}{Z_{line}}\right)\cos(\phi - \theta) \tag{3}$$

Using Eq. (3) in (2), I can be formulated as,

$$I = \frac{1}{\sqrt{A}}\frac{E}{Z_{line}} \tag{4}$$

Therefore, the magnitude of the load voltage can be found using,

$$V = IZ_{load} = \frac{1}{\sqrt{A}}\frac{Z_{load}}{Z_{line}}E \tag{5}$$

Hence, the real and reactive power of the load can be expressed by,

$$P_R = VI\cos\theta = \frac{Z_{load}}{A}\left(\frac{E}{Z_{line}}\right)^2\cos\theta \tag{6}$$

$$Q_R = VI\sin\theta = \frac{Z_{load}}{A}\left(\frac{E}{Z_{line}}\right)^2\sin\theta \tag{7}$$

The relationship between reactive power Q_R and the load voltage V by keeping P_R constant can be determined using (6) and (7). This relationship provides the Q-V curve of a load bus as depicted in Fig. 1. However, Jacobian matrix tends to be singular in the vicinity of voltage collapse point. Therefore, it becomes numerically complicated to obtain a power flow solution near the bottom of the Q-V curve. To resolve this challenge, continuation power flow technique is used to achieve a complete Q-V curve. Note that this method provides power flow solutions near or at the voltage collapse point [31].

B. PROPOSED LOAD SHEDDING SCHEME

At first, reactive power margins for all P-Q buses are calculated using the procedures mentioned in previous subsections. To preserve voltage stability, greater amount of load needs to be shed at weaker buses. As mentioned earlier, a lower reactive power margin indicates a weaker bus. Therefore, inverse values of reactive power margins are determined. Then, these values are normalized to calculate an index called reactive margin factor. Let, N be the number of load buses and $Q_{m1}, Q_{m2}, \ldots, Q_{mN}$ be the inverse of reactive power margins of load bus-1 to load bus-N respectively. Thus, reactive margin factor of i-th load bus (r_i) can be calculated using (8).

$$r_i = \frac{Q_{mi}}{Q_{m1} + Q_{m2} + \cdots + Q_{mN}} = \frac{Q_{mi}}{\sum_{j=1}^{N} Q_{mj}} \tag{8}$$

The proposed scheme consists of multiple stages. Each stage comes into action when system frequency collapses beneath a certain threshold. Assume that there are n numbers of stages in the scheme. Thus, in the first stage, the amount of load shedding incurred by i-th load bus ($LS_{i,1}$) is calculated as follows.

$$LS_{i,1} = r_i \times L_i \tag{9}$$

where L_i is the total load of i-th bus.

In the second stage, the load shedding amount of i-th load bus is determined using Eq. (20) considering the fact that a certain portion of load is already cut in the first stage.

$$LS_{i,2} = (1 - r_i) \times r_i \times L_i = (r_i - r_i^2) \times L_i \tag{10}$$

Similarly, in the third stage, the load shedding at i-th bus is computed as follows.

$$LS_{i,3} = [1 - r_i - (r_i - r_i^2)] \times r_i \times L_i = (r_i - 2r_i^2 + r_i^3) \times L_i \tag{11}$$

In the fourth stage, the load shedding at i-th bus is given by,

$$\begin{aligned} LS_{i,4} &= [1 - r_i - (r_i - r_i^2) - (r_i - 2r_i^2 + r_i^3)] \times r_i \times L_i \\ &= (r_i - 3r_i^2 + 3r_i^3 - r_i^4) \times L_i \end{aligned} \tag{12}$$

Likewise, in the fifth stage, the load sheeding amount at i-th bus can be found from Eq. (24).

$$\begin{aligned} LS_{i,5} &= [1 - r_i - (r_i - r_i^2) - (r_i - 2r_i^2 + r_i^3) \\ &\quad - (r_i - 3r_i^2 + 3r_i^3 - r_i^4)] \times r_i \times L_i \end{aligned} \tag{13}$$

$$LS_{i,5} = (r_i - 4r_i^2 + 6r_i^3 - 4r_i^4 + r_i^5) \times L_i \tag{14}$$

In the sixth stage, the qunatity of load shedding at i-th bus is evaluated as follows.

$$\begin{aligned} LS_{i,6} &= [1 - r_i - (r_i - r_i^2) - (r_i - 2r_i^2 + r_i^3) \\ &\quad - (r_i - 3r_i^2 + 3r_i^3 - r_i^4) - (r_i - 4r_i^2 + 6r_i^3 \\ &\quad - 4r_i^4 + r_i^5)] \times r_i \times L_i \end{aligned} \tag{15}$$

$$LS_{i,6} = (r_i - 5r_i^2 + 10r_i^3 - 10r_i^4 + 5r_i^5 - r_i^6) \times L_i \tag{16}$$

It is noticed that the coefficients of equations used to represent load shedding amounts follow the Pascal's triangle [32]. Pascal's triangle is an array, which is formed by adding adjacent elements in previous rows. Essentially, this triangle comprises the values of binomial coefficients. Therefore, in the n-th stage, the amount of load shedding encountered by i-th load bus can be expressed using (17).

$$LS_{i,n} = (1 - r_i)^{n-1} \times r_i \times L_i \tag{17}$$

Hence, the load shedding factor of i-th bus in the n-th stage ($LF_{i,n}$) is given by (18).

$$LF_{i,n} = (1 - r_i)^{n-1} \times r_i \tag{18}$$

It is pointed out that usually reactive power margin of a load bus decreases with increase in total demand [33]. In the proposed method, normalization is done while calculating the reactive margin factor of all load buses. Thus, the impact of load variation does not significantly affect the values of reactive margin factor. Therefore, the load shedding factors determined in a specific load level can be generally used for other load conditions. The numerical results presented in section 4 also conform to this proposition.

C. STEPS FOR IMPLEMENTATION

The proposed load shedding scheme is determined offline while it performs online. However, it can adapt to system load variation as mentioned in the previous sub-section. Particularly, UFLS relays need to be set to shed different percentage of load using load shedding factor. Thus, the proposed technique is practically implementable. Fig. 3 depicts a flow chart to implement the developed scheme. Also, the steps are briefly mentioned below.

Step-1: For all P-Q buses, calculate the reactive power margins.

Step-2: Calculate the inverse values of reactive power margins of all load buses.

Step-3: Normalize above values to calculate the reactive margin factors of all load buses using (8).

Step-4: Set UFLS relays for all load buses using load shedding factors calculated via (18).

Step-5: Following a contingency, check if system frequency (f) crosses the 1st UFLS threshold (f_{th1}). If yes, shed $LS_{i,1}$ amount of load quantified by (9) from i-th load bus. If no, do not apply any load shedding.

Step-6: Check if system frequency (f) crosses the 2nd UFLS threshold (f_{th2}). If yes, shed $LS_{i,2}$ amount of load quantified by (10) from i-th load bus. If no, do not apply any load shedding.

Step-7: Check if system frequency (f) crosses the n-th UFLS threshold (f_{thn}). If yes, shed $LS_{i,n}$ amount of load quantified by (17) from i-th load bus. If no, do not apply any load shedding.

Step-8: When frequency excursion is eventually stopped, conclude the load shedding process.

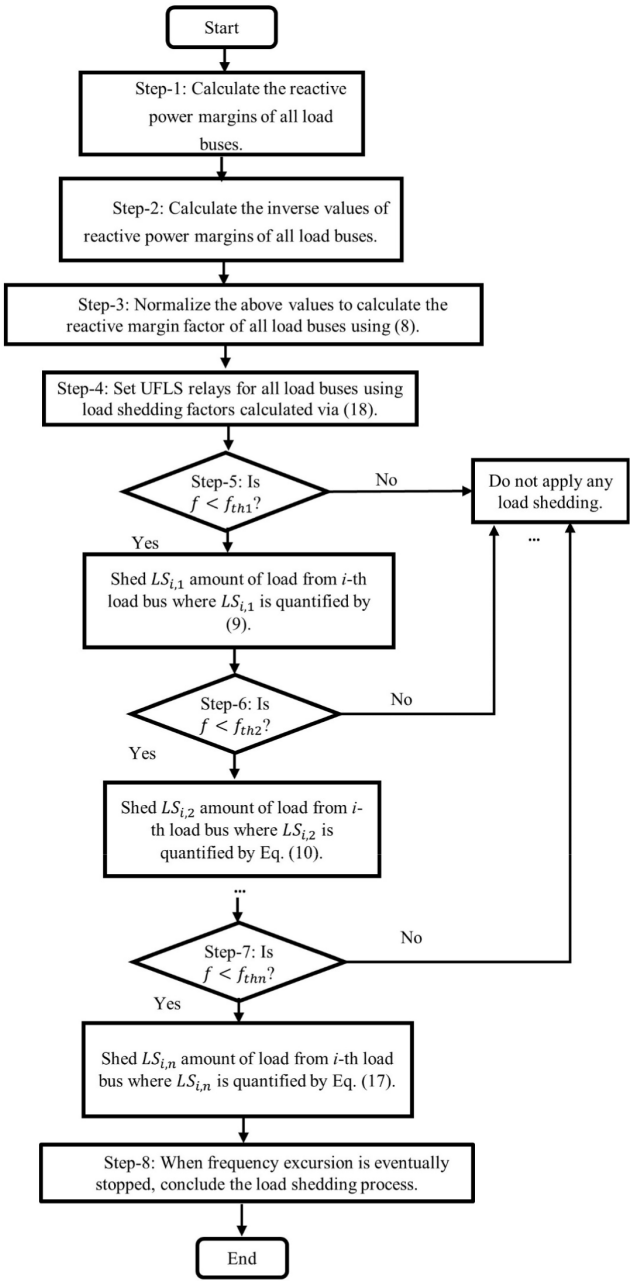

FIGURE 3. Implementation steps of the developed method.

III. STUDIED GRID AND SIMULATION OUTLINE

A. TEST NETWORK

The simulated grid is constructed based on the of South East Australia 14-Generator Model [34]. The network diagram of the studied grid is illustrated in Fig. 4. The system consists of 59 buses and five interconnected areas.

Area-5 specifies the low inertia network, which is an equivalent representation of South Australia's high- voltage transmission network. As South Australia has one of the highest wind penetration levels compared to its demand in the world [35], it can be treated as a typical example of a low inertia wind dominated power system. Area-5 is connected to Area-3 (denotes the neighboring state Victoria) via a high voltage AC interconnection. The total wind power generation capacity in Area-5 is around 1,800 MW [36]. Due to this significant installed wind capacity, the number of fossil-fueled power plants has been considerably reduced in recent times. At present, there are only two major power plants. These are TPS_5 (Torrens Island Power Station) and PPS_5 (Pelican Point Power Station). Each power plant has multiple synchronous generating units. Table 1 contains the necessary information regarding the conventional power plants.

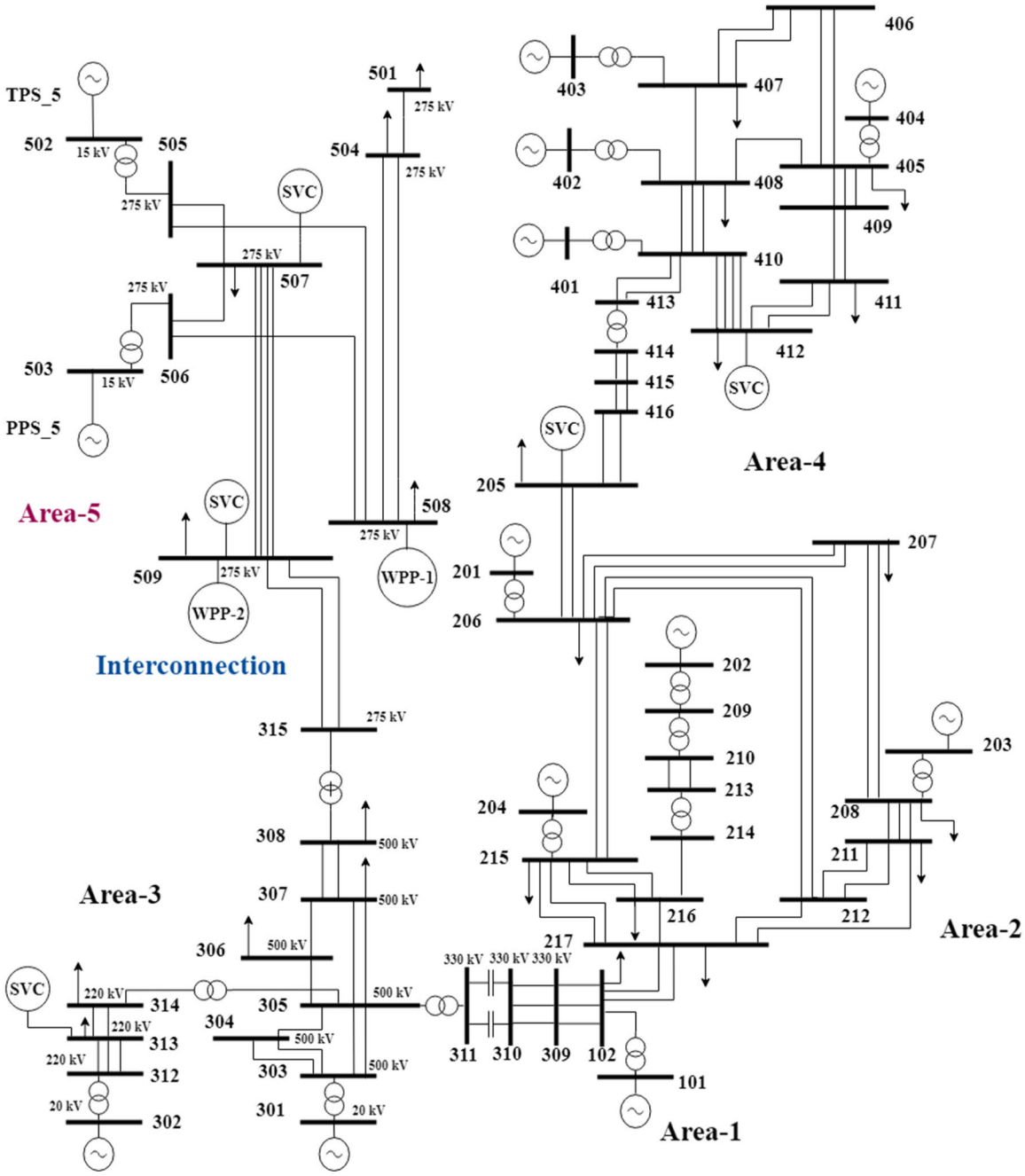

FIGURE 4. Single-line diagram of simulated power system.

TABLE 1. Information regarding conventional power plants.

Power plant name	Number of units	Unit capacity (MW)	Unit MVA rating	Unit inertia constant (s)
TPS_5	4	200	250	4.0
PPS_5	6	150	166	7.5

In this paper, wind power plants (WPPs) are aggregated according to geographical sites, and then connected to two buses – 508 and 509 in the simulation network. For dynamic simulations, all the wind power plants are modeled using type-3 WTGs.

It is worth mentioning that South Australia has around 1500 MW of distributed photovoltaic (PV) generation [36], [37]. These PV sources are treated as behind the meter mode, i.e. net load excluding PV generation is catered by synchronous and wind power plants. Therefore, distributed PV generation is not taken into account in this paper.

TABLE 2. Outline of simulation scenarios.

Case study	No. of online synchronous generators	Inertia (MWs)	Synchronous generation (MW)	Wind generation (MW)	Interconnection import (MW)
1	5	5500	719	650	550
	4	4500	586	800	
	3	3500	448	950	
2	5	5500	721	550	650
	4	4500	589	700	
	3	3500	449	850	

B. SIMULATION SCENARIOS

To investigate the worst case scenario, loss of interconnection during power import to Area-5 from Area-3 is considered as a contingency. Under such cases, Area-5 becomes islanded and it has to depend on its limited number of online synchronous machines and available load shedding mechanism to control frequency. In this paper, two simulation cases are considered to analyze frequency response. These are – loss of an interconnection importing 550MW (case study-1) and loss of 650 MW interconnection import (case study-2). To emulate the low system inertia conditions, the number of online conventional synchronous machines is step-wise varied from 5 to 3 in both cases. The total load in Area-5 is kept unchanged at 1,800 MW throughout the study. Wind generation is changed from 650 to 950 MW. It results in a wind penetration level of 28.63% to 48.77%. The simulation scenarios are summarized in Table 2. Note that the total system inertia (*IR* in MWs) is calculated using (19).

$$IR = \sum_{j=1}^{j=N_C} (S_j \times H_j) \tag{19}$$

where S_j refers to the MVA rating of j-th synchronous generator, H_j is the inertia constant of j-th synchronous generator (ins) and N_C denotes the total number of online synchronous generators.

All the modeling and simulations are performed in PSS®E software [38]. This power system simulation platform is extensively utilized in industry and academia to execute power system dynamic studies. To explore the effectiveness of the proposed scheme in conservative conditions, variation in frequency due to load damping is ignored.

IV. RESULTS AND ANALYSES

A. EVALUATION OF LOAD SHEDDING FACTORS

Load shedding factors are enumerated assuming that the proposed load shedding scheme comprises three stages. In the test network, there are four load buses viz. 504, 507, 508 and 509. The reactive power margins of all P-Q buses are determined from the corresponding Q-V curves. The reactive margin factors are calculated using (8) during 1800 MW load condition (with 5 online synchronous generators and 550 MW interconnection import). The values are shown in Table 3. It is apparent that bus 509 has the lowest reactive power margin. Consequently, it should incur higher percentage of load shedding compared to other buses.

TABLE 3. Reactive margin factors of load buses during 1800 MW load.

Bus ID	Reactive power margin (MVAr)	Reactive power margin (p.u. on 100 MVA system base)	Inverse of reactive power margin (p.u.)	Reactive margin factor
504	745.08	7.45	0.1342	0.1735
507	648.10	6.48	0.1543	0.1995
508	874.04	8.74	0.1144	0.1479
509	270.73	2.70	0.3703	0.4789

TABLE 4. Load shedding factors of load buses during 1800 MW load.

Bus ID	Load shedding factor (%)		
	1st stage	2nd stage	3rd stage
504	17.35	14.33	11.85
507	19.95	15.96	12.78
508	14.79	12.60	10.73
509	47.89	24.95	13.00

TABLE 5. Load shedding factors of load buses during 1600 MW load.

Bus ID	Load shedding factor (%)		
	1st stage	2nd stage	3rd stage
504	17.37	14.34	11.87
507	19.96	15.97	12.79
508	14.80	12.62	10.74
509	47.91	24.96	13.01

TABLE 6. Load shedding factors of load buses during 2000 MW load.

Bus ID	Load shedding factor (%)		
	1st stage	2nd stage	3rd stage
504	17.34	14.32	11.84
507	19.94	15.95	12.77
508	14.77	12.58	10.71
509	47.87	24.94	12.99

According to the reactive margin factors, load shedding factors are evaluated using (18). The values of three stages are provided in Table 4. It is evident that the proportion of load shedding changes depending on bus strength.

To explore the adaptability of the proposed method in different operating conditions, two additional load levels – 1600 MW and 2000 MW are considered. Synchronous generation, wind generation and interconnection import are adjusted to meet the load. The load shedding factors are re-calculated, which are provided in Tables 5 and 6 respectively.

It is apparent from the above tables that the load shedding factors remains almost unchanged with the change of system load. Therefore, the load shedding factors calculated in a typical load scenario can be used for other operating conditions.

B. FREQUENCY RESPONSE ANALYSIS

Performances of the proposed algorithm are explored via two different UFLS settings. Here, the term ''UFLS setting'' refers to the frequency thresholds at which the load shedding stages are activated. In the 1st UFLS setting, the frequency thresholds are assumed to be 49.25 Hz, 48.75 Hz

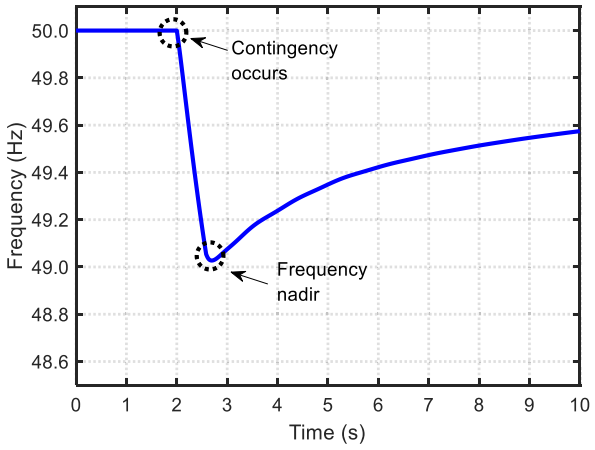

FIGURE 5. System frequency response following 550 MW interconnection trip for 1st UFLS setting in 5 machines case.

and 48.25 Hz. It means the 1st stage of load shedding is triggered when system frequency falls below 49.25 Hz and so on. Meanwhile, in the 2nd UFLS setting, the frequency thresholds are set as 49 Hz, 48.50 Hz and 48 Hz.

Following the interconnection trip, frequencies of online synchronous machines are recorded. After that, Center of Frequency (COF) (f) is estimated via (20). This equation is utilized to remove meager variations amongst different synchronous machines.

$$f = \frac{\sum_{j=1}^{j=N_C} (f_j \times S_j \times H_j)}{\sum_{j=1}^{j=N_C} (S_j \times H_j)} \tag{20}$$

where f_j delineates the instantaneous frequency of j-th synchronous generator (in Hz).

1) PERFORMANCE OF THE PROPOSED SCHEME IN CASE STUDY-1

In this case, the loss of 550 MW interconnection is simulated. The proposed scheme is implemented using the 1st UFLS setting. After the interconnection trip, the system frequency starts to decline. When it falls below 49.25 Hz, the 1st stage of the load shedding scheme is activated. Likewise, depending on the frequency excursion, the other stages are subsequently enabled.

The frequency response curve for 5 machines case is depicted in Fig. 5. From the figure, it can be inferred that the frequency decline is successfully stopped at 49.05 Hz. Therefore, only the 1st stage of load shedding is triggered, which causes a total load cut of 355 MW.

When the number of online synchronous machine reduces, the system frequency response deteriorates. As such, in 4 machines and 3 machines cases, the frequency nadirs are found to be 48.90 Hz and 48.76 Hz respectively. The frequency response curves are illustrated in Fig. 6 and Fig. 7. In both conditions, the network encounters a total of 355 MW

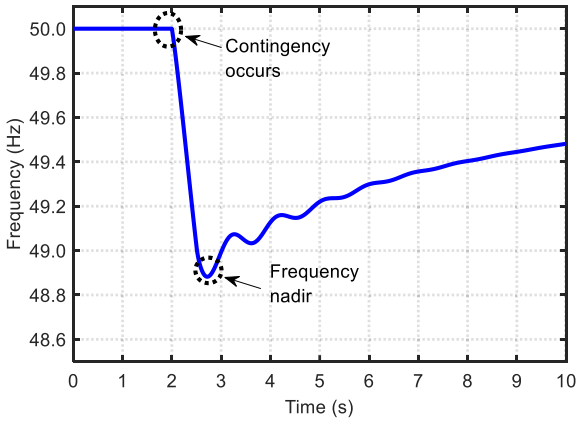

FIGURE 6. System frequency response following 550 MW interconnection trip for 1st UFLS setting in 4 machines case.

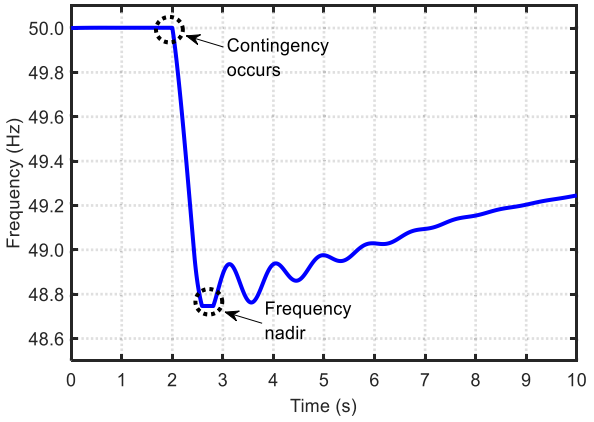

FIGURE 7. System frequency response following 550 MW interconnection trip for 1st UFLS setting in 3 machines case.

load shedding due to the activation of only one stages in the load shedding scheme.

The above simulations are re-executed using the proposed load shedding mechanism for the 2nd UFLS setting. In this setting, the frequency nadirs become 48.80 Hz, 48.71 Hz and 48.51 Hz in 5 machines, 4 machines and 3 machines cases accordingly. Also, the 1st stage of load shedding is instigated, which results in a total load cut of 355 MW in all three cases. For better observation, frequency excursion curves are illustrated in Fig. 8, Fig. 9 and Fig. 10.

It is evident from the above simulations that the proposed scheme satisfactorily rescues the system frequency following the loss of 550 MW interconnection. In addition, frequency response performance improves when higher UFLS thresholds are used (i.e. 1st setting). However, for both UFLS settings, the amount of load shedding is found to be equal.

2) PERFORMANCE OF THE PROPOSED SCHEME IN CASE STUDY-2

In this case, a more severe contingency of 650 MW interconnection trip is applied. The proposed load shedding scheme is examined for two UFLS settings as depicted in the previous

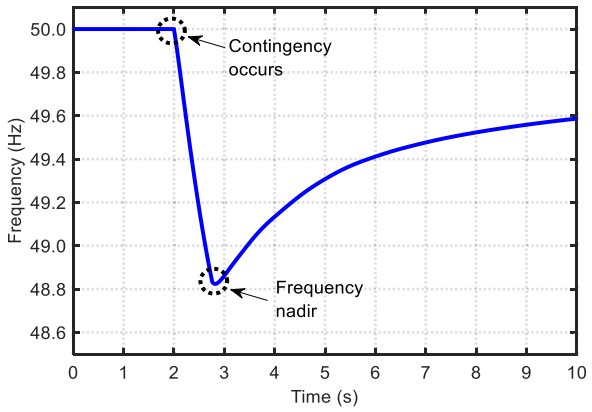

FIGURE 8. System frequency response following 550 MW interconnection trip for 2nd UFLS setting in 5 machines case.

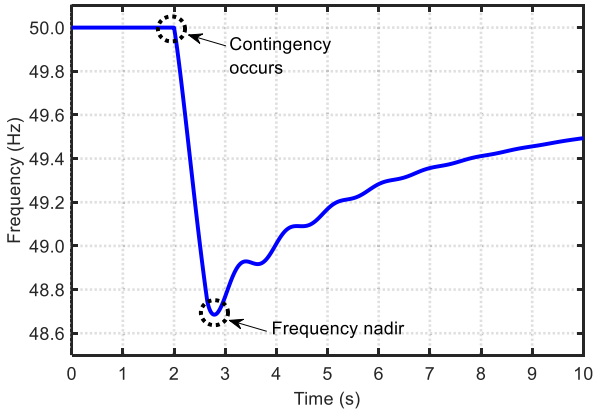

FIGURE 9. System frequency response following 550 MW interconnection trip for 2nd UFLS setting in 4 machines case.

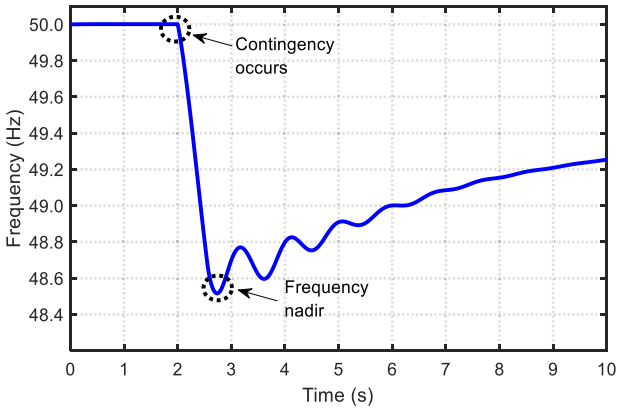

FIGURE 10. System frequency response following 550 MW interconnection trip for 2nd UFLS setting in 3 machines case.

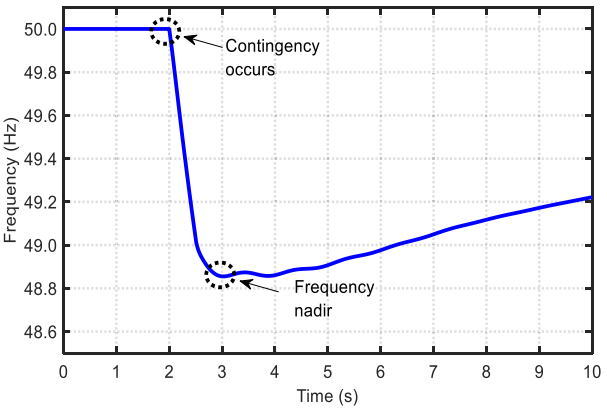

FIGURE 11. System frequency response following 650 MW interconnection trip for 1st UFLS setting in 5 machines case.

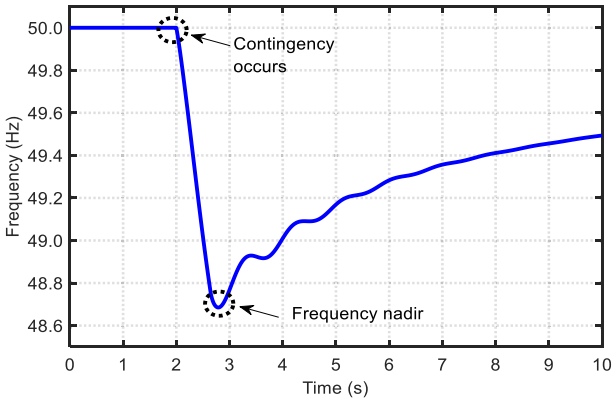

FIGURE 12. System frequency response following 650 MW interconnection trip for 1st UFLS setting in 4 machines case.

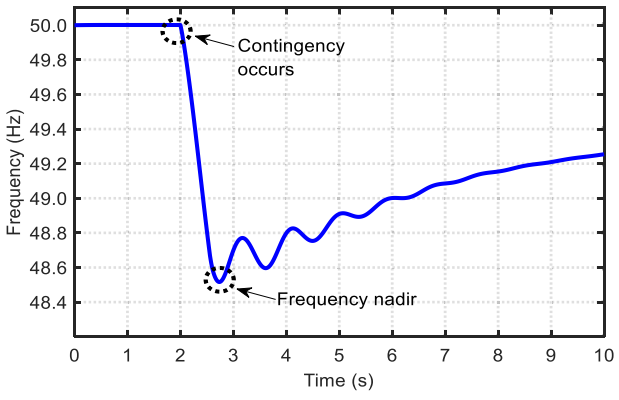

FIGURE 13. System frequency response following 650 MW interconnection trip for 1st UFLS setting in 3 machines case.

sub-section. In the 1st setting, the proposed technique successfully arrests the frequency excursion at 48.85 Hz in 5 machines case. Therefore, only the 1st stage of the load shedding scheme is deployed. It causes a total load cut of 355 MW.

Furthermore, the frequency nadirs are found to be 48.73 in 4 machines and 48.52 Hz in 3 machines cases. Also, two stages of load shedding are activated for these scenarios. Therefore, the network faces around 505 MW load shedding. The Frequency response curves under various operating conditions are presented in Fig. 11, Fig. 12 and Fig. 13.

For the 2nd UFLS setting, the network frequency deviation increases (compared to the 1st setting). Consequently, the frequency nadirs become 48.70 Hz, 48.49 Hz and 48.38 Hz when

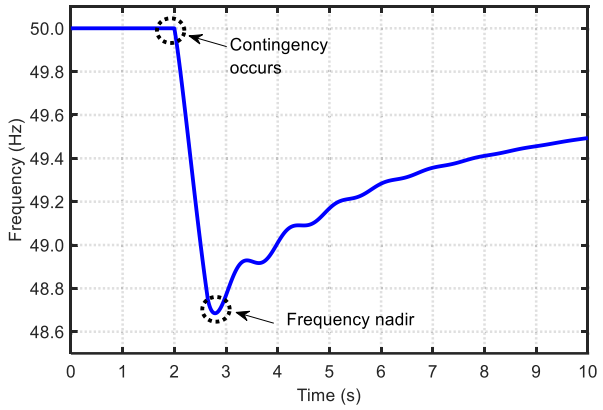

FIGURE 14. System frequency response following 650 MW interconnection trip for 2nd UFLS setting in 5 machines case.

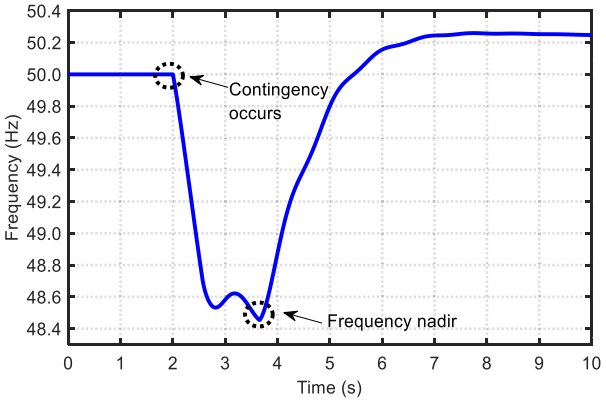

FIGURE 15. System frequency response following 650 MW interconnection trip for 2nd UFLS setting in 4 machines case.

5 machines, 4 machines and 3 machines are committed. Frequency response curves are depicted in Fig. 14, Fig. 15 and Fig. 16. In 5 machines case, the 1st stage of load shedding is triggered. However, in 4 machines and 3 machines case, 1st and 2nd stages of load shedding are enabled. Therefore, the network encounters 355 MW load cut in the 5 machines case, whereas 505 MW load is shed in both 4 machines and 3 machines cases.

It can be inferred from the above analyses that proposed scheme successfully retains system frequency following an acute contingency such as the interconnection trip. As a result, the network does not encounter any blackout even in a very low inertia operating condition (e.g. loss of 650 MW interconnection during 3 machines case). Also, voltage stability is retained by proportionally applying higher amount of load shedding to weaker buses. Therefore, the proposed scheme can be utilized in a low inertia grid to enhance frequency resilience during prolific wind renewable penetration.

C. VALIDATION OF THE PROPOSED SCHEME

To validate the proposed load shedding technique, its effectiveness is thoroughly compared with a conventional UFLS scheme. The conventional UFLS also includes several stages.

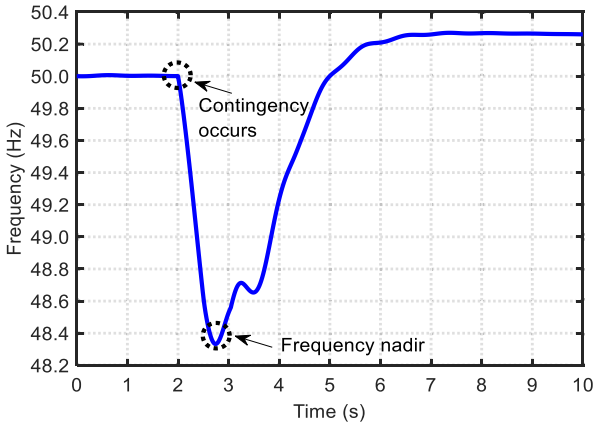

FIGURE 16. System frequency response following 650 MW interconnection trip for 2nd UFLS setting in 3 machines case.

In a specific stage, equal percentage of load is shed from all load buses when the frequency collapses beyond a certain threshold. Assume that there are m numbers of stages in the conventional UFLS scheme. The stages are configured to cut $d_1, d_2, d_3, \ldots, d_m$ percent of the load from each bus in the 1st, 2nd, 3rd, ….. m-th stage respectively. Therefore, in the m-th stage, the amount of load shedding incurred by k-th load bus can be obtained from (21).

$$LS_{k,m} = d_m \times L_k \tag{21}$$

where L_k is the original load of k-th bus (in MW).

In this paper, the traditional UFLS scheme is assumed to have three stages to shed 50% of the total load. To activate the scheme, two UFLS settings as mentioned in the section 4.B are separately utilized. The effectiveness of the proposed and conventional load shedding techniques is compared as follows.

1) PERFORMANCE COMPARISON IN CASE STUDY-1

Frequency response is analyzed using the conventional UFLS technique following the loss of 550 MW interconnection. In the 1st UFLS setting (frequency thresholds are: 49.25 Hz, 48.75 and 48.25 Hz), the frequency nadirs are determined to be 48.72 Hz, 48.66 Hz and 48.50 Hz in 5 machines, 4 machines and 3 machines cases respectively. However, the corresponding frequency nadirs are 49.05 Hz, 48.90 Hz and 48.76 Hz when the proposed scheme is deployed. Therefore, the system frequency nadirs improve by 0.33 Hz, 0.24 Hz and 0.26 Hz in various operating conditions by using the proposed technique. Also, the amount of load shedding in all three cases is 530 MW for the conventional UFLS. On the other hand, the proposed scheme results in a load cut of 355 MW. Thus, the quantity of load shedding reduces by 175 MW in all cases when the proposed scheme is utilized. Figs. 17, 18 and 19 show the comparison of frequency response between the proposed and the conventional load shedding algorithms under various conditions.

For the 2nd UFLS setting (i.e. at 49 Hz, 48.50 Hz and 48 Hz thresholds), the conventional UFLS provides the frequency

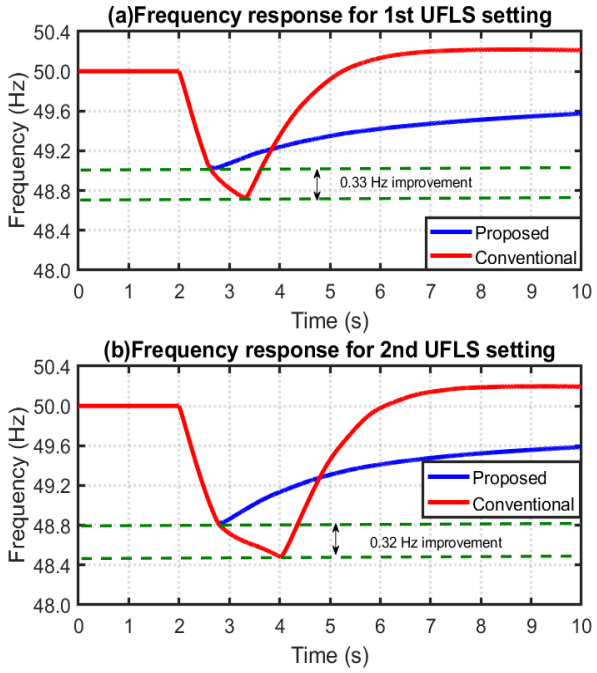

FIGURE 17. Frequency response comparison between proposed and conventional schemes due to 550 MW interconnection trip in 5 machines case.

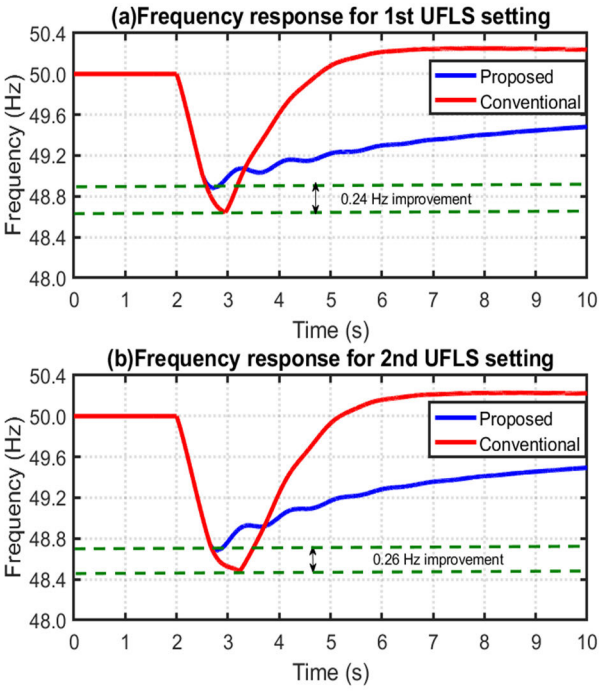

FIGURE 18. Frequency response comparison between proposed and conventional schemes due to 550 MW interconnection trip in 4 machines case.

nadirs of 48.48 Hz, 48.45 Hz and 48.37 Hz in 5 machines, 4 machines and 3 machines cases respectively. The corresponding frequency nadirs are 48.80 Hz, 48.71 Hz and 48.51 Hz while the proposed scheme is in place. Thus, the

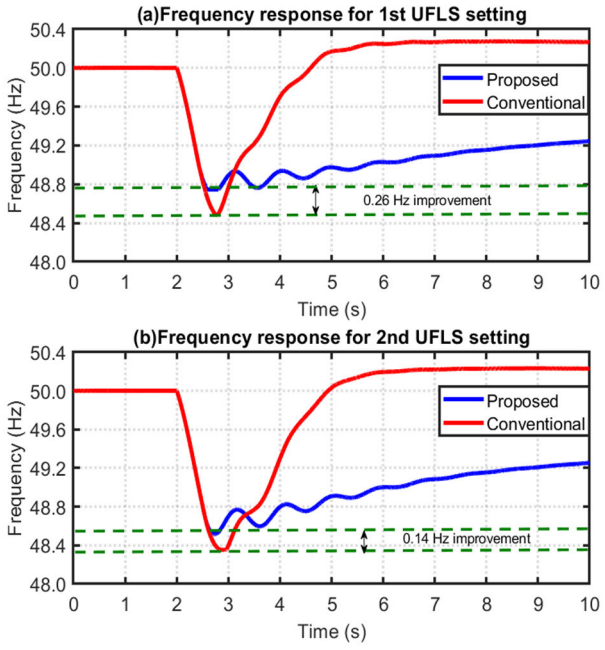

FIGURE 19. Frequency response comparison between proposed and conventional schemes due to 550 MW interconnection trip in 3 machines case.

frequency nadirs enhance by 0.32 Hz, 0.26 Hz and 0.14 Hz for the different number of committed synchronous machines. Similar to the previous scenario, load shedding decreases by 175 MW in all simulation cases when the proposed scheme is used.

2) PERFORMANCE COMPARISON IN CASE STUDY-2

In this case, 650 MW interconnection trip is simulated. In the 1st UFLS configuration, the conventional technique yields frequency nadirs of 48.65 Hz, 48.52 Hz and 48.32 Hz during 5 machines, 4 machines and 3 machines cases respectively. In contrast, the corresponding frequency nadirs are found to be 48.85 Hz, 48.73 Hz and 48.52 Hz after deploying the proposed mechanism. Thus, the frequency nadirs improve by 0.20 Hz, 0.21 Hz and 0.20 Hz in different simulation cases. Furthermore, the network encounters a total of 530 MW load shedding with the traditional UFLS scheme in all cases. However, in 5 machines condition, the amount of load shedding is only 355 MW using the proposed technique. In addition, the load shedding amount is 505 MW in 4 machines and 3 machines case. Therefore, load shedding decreases by 175 MW in 5 machines case when the proposed scheme is utilized. In 4 machines and 3 machines, the reduction in load shedding is 25 MW.

For the 2nd set of UFLS thresholds, the conventional scheme stops the frequency excursion at 48.40 Hz, 48.34 Hz and 48.12 Hz in 5 machines, 4 machines and 3 machines cases respectively. On the contrary, the frequency decline is arrested at 48.70 Hz, 48.49 Hz and 48.38 Hz while the proposed scheme is in place. Therefore, the frequency nadirs improve by 0.30 Hz, 0.15 Hz and 0.26 Hz under the different

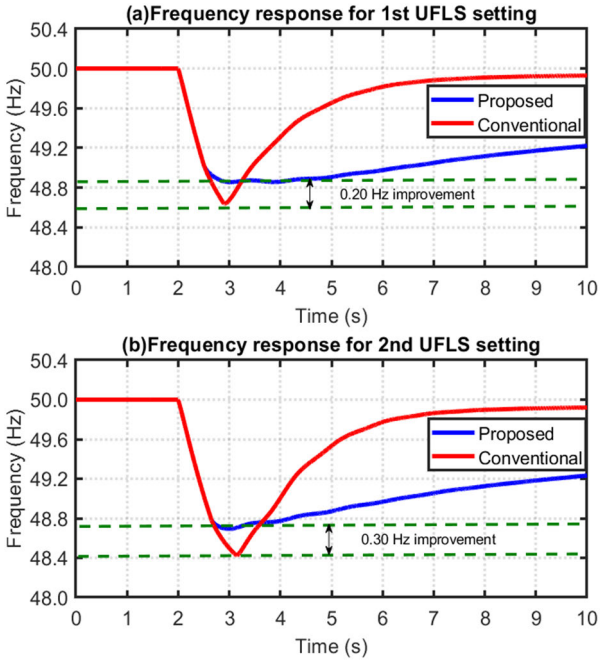

FIGURE 20. Frequency response comparison between proposed and conventional schemes due to 650 MW interconnection trip in 5 machines case.

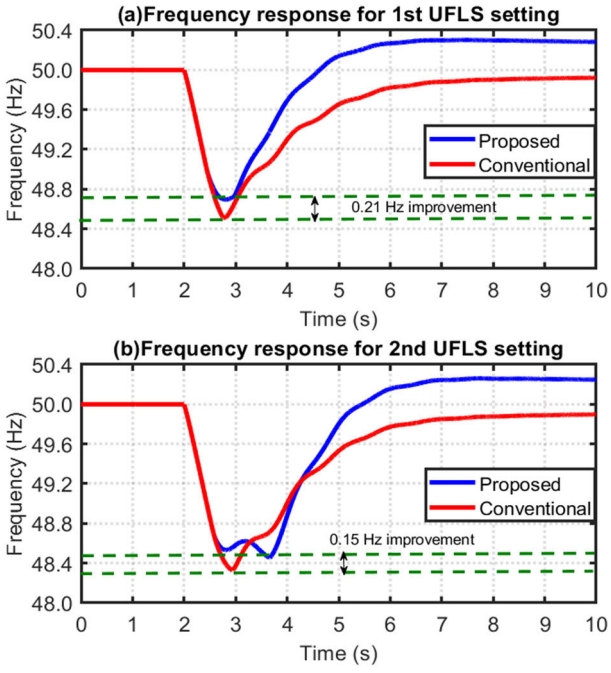

FIGURE 21. Frequency response comparison between proposed and conventional schemes due to 650 MW interconnection trip in 4 machines case.

situations. In addition, the reduction of load shedding via the proposed scheme is same as that of the 1st UFLS setting (i.e. 175 MW in 5 machines case, and 25 MW in 4 machines and 3 machines case). Figs. 20, 21 and 22 illustrate the comparison of frequency response between the proposed and the conventional load shedding methods in different scenarios.

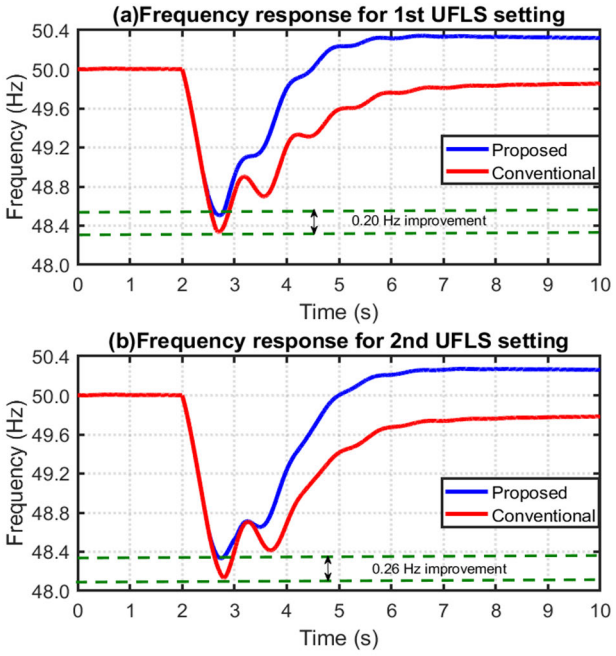

FIGURE 22. Frequency response comparison between proposed and conventional schemes due to 650 MW interconnection trip in 3 machines case.

TABLE 7. Performance summary of proposed load shedding scheme.

Contingency	No. of online synchronous generators	Improvement of frequency nadir (Hz)		Reduction of load shedding (MW)	
		1st UFLS setting	2nd UFLS setting	1st UFLS setting	2nd UFLS setting
550 MW interconnection trip	5	0.33	0.32	175	175
	4	0.24	0.26	175	175
	3	0.26	0.14	175	175
650 MW interconnection trip	5	0.20	0.30	175	175
	4	0.21	0.15	25	25
	3	0.20	0.26	25	25

It is evident from these investigations that the proposed scheme yields superior frequency response than that of the traditional UFLS strategy in all simulation cases. Also, the amount of load shedding reduces when the proposed scheme is deployed. Therefore, the proposed load shedding strategy is more competent compared to the conventional UFLS technique. For better observation, superiority of the proposed scheme is summarized in Table 7.

In this paper, high penetration of wind generation is considered while studying the performance of the proposed scheme. Like variable speed WTGs, the utility-scale PV generators usually do not participate in frequency regulation unless additional control strategy is adopted. Hence, from frequency response point of view, both wind and PV generators exhibit similar behavior. Therefore, the proposed methodology is also applicable to PV dominated low inertia grids.

V. DISCUSSIONS

A. SCALABILITY OF THE PROPOSED APPROACH

The scalability of the proposed approach can be discussed from two different viewpoints viz., from network perspective

and from load variation perspective. For a large network, the number of load buses increases. Thus, to apply the proposed approach, reactive power margins of all of the load buses need to be determined to further obtain the load shedding factors. Note that the load shedding factors are determined offline before implementation. Therefore, the recalculations of load shedding factors of all load buses have to be performed only once. It implies that the proposed methodology can easily be scaled-up for a large power system.

In addition, for load variations in a certain network, the load shedding factors remain almost unchanged (refer to Tables 4, 5 and 6). This is due to the fact that in this method, normalized reactive margin factors are taken into account while calculating the load shedding factors. Consequently, the proposed methodology successfully adapts to the various load levels. In other words, the proposed approach is scalable for various load conditions in a given network.

B. CONTROLLING PARAMETERS

The main controlling parameters of the proposed scheme are load shedding factors and UFLS activation thresholds. The load shedding factors are sensitive to the reactive margin factors. These factors are functions of reactive power margins of load buses. Reactive power margins depend on system load, load bus voltages and corresponding line reactances. Usually, the line reactances are known to a system operator. In a given load condition, voltages of load buses can be obtained from load flow solutions. It is worth mentioning that load shedding factors are eventually determined from normalized reactive margin factors. Therefore, load shedding factors of different load buses are almost unchanged in a specific network under various load conditions. However, if a network is augmented by adding new lines, buses etc., load shedding factors need to be recalculated.

In addition, UFLS activation thresholds of different stages can be chosen by a system operator according to the standard practices. It may depend on the size of the largest possible contingency and renewable penetration level. In this paper, two sets of typical values are presumed to activate various stages of the UFLS scheme. It is found that with similar settings, the proposed approach provides better results compared to the conventional scheme.

C. COMPUTATIONAL BURDEN

The computational burden for the proposed method consists of two parts viz. time to calculate reactive power margin and time to execute dynamic simulation. In this work, a computer with the following specification is used: Intel®core™ i5-8250 CPU@ 1.7-3.4 GHz. This computer takes around 763 ms to determine the reactive power margin of a load bus. In addition, the above computer needs approximately 1.3 s to complete a dynamic simulation in PSS®E software. For a large network, deployment of a high configuration computer would be able to minimize the computational cost.

D. LIMITATIONS AND PRACTICAL APPLICABILITY

The limitations of the proposed methodology are as follows.

(i) Rate of change of frequency (ROCOF) is not considered while activating the proposed load shedding scheme.

(ii) UFLS activation thresholds are fixed, which are under the jurisdiction of a network operator. In other words, thresholds are not being dynamically changed based on the contingency size.

The above aspects will be considered in the future work.

In addition, a practical power system would be relatively larger. Such a system usually contains high number of load buses. Hence, to implement the proposed methodology, reactive power margins of all of the load buses have to be calculated to further determine the load shedding factors. Note that the load shedding factors are computed offline before implementation. Therefore, the recalculations of load shedding factors have to be performed only once. Also, the load shedding factors remain almost unchanged in various load levels due to the adaptable nature of the developed technique. Thus, the UFLS relays have to be set for once until the network is augmented. Therefore, the proposed algorithm can easily be extended in practical applications.

VI. CONCLUSION

In this research work, a frequency and voltage stability based load shedding mechanism is developed to improve the frequency resilience of low inertia power systems in presence of high wind power penetration. The vast majority of the existing works describe centralized and measurement based load shedding techniques. These techniques may not perform well in a large network due to communication delay and lack of widespread deployment of PMU units in practical power systems. To address this issue, an approach is presented in this paper, which does not require any high-speed communication infrastructure and PMU. Particularly, higher percentage of load shedding is applied to relatively weaker buses to concurrently retain voltage and frequency stabilities following a contingency. To this end, a general expression of load shedding amount, which follows Pascal's triangle rule, is formulated based on reactive power margin. Also, the impact of network load variation is taken care of in the developed method. Notably, the proposed algorithm is scalable and implantable in large-scale practical power networks. In addition, the computational burden for execution of the developed technique is minimal.

The competency of the proposed method is investigated due to the loss of an interconnection in a low inertia network using two different UFLS settings. It is found that during 550 MW interconnection trip, the frequency nadirs are 49.05 Hz, 48.90 and 48.76 Hz in 5 machines, 4 machines and 3 machines cases respectively in the 1st UFLS setting. Meanwhile for the 2nd UFLS setting, the corresponding nadirs are found to be 48.80 Hz, 48.71 and 48.51 Hz. Also, in both settings, the network encounters a total load

shedding of 355 MW. Furthermore, subsequent to the trip of 650 MW interconnection, the frequency excursion is stopped at 48.85 Hz, 48.73 Hz and 48.52 Hz in 5 machines, 4 machines and 3 machines cases respectively for the 1st UFLS thresholds. In addition, if the 2nd UFLS setting is in place, the frequency nadirs become 48.70 Hz, 48.49 Hz and 48.38 Hz. Under both UFLS configurations, the amount of load shedding is 355 MW in 5 machines case; however, it increases to 505 MW when 4 machines and 3 machines are committed. The simulation results thus reveal that the proposed load shedding algorithm ensures satisfactory frequency response under high wind power penetration.

To validate the proposed scheme, system performance is compared to that of a conventional UFLS scheme. It is noticed that in all cases, frequency nadirs considerably improve when the proposed scheme is utilized. In addition, the network encounters less amount of load cut. Therefore, it is evident that the developed load shedding scheme provides superior frequency stability than the conventional one. Finally, it is worth mentioning that the proposed scheme is generic in nature. Thus, it is applicable to any power systems to enhance frequency response by preserving voltage stability, especially during prolific penetration of non-synchronous renewable resources.

REFERENCES

[1] Y. Xie, C. Li, H. Zhang, H. Sun, and V. Terzija, "Long-term frequency stability assessment based on extended frequency response model," *IEEE Access*, vol. 8, pp. 122444–122455, 2020.

[2] E. Rakhshani, D. Gusain, V. Sewdien, J. L. R. Torres, and M. A. M. M. Van Der Meijden, "A key performance indicator to assess the frequency stability of wind generation dominated power system," *IEEE Access*, vol. 7, pp. 130957–130969, 2019.

[3] D. Ortiz-Villalba, C. Rahmann, R. Alvarez, C. A. Canizares, and C. Strunck, "Practical framework for frequency stability studies in power systems with renewable energy sources," *IEEE Access*, vol. 8, pp. 202286–202297, 2020.

[4] M. Khamies, G. Magdy, M. E. Hussein, F. A. Banakhr, and S. Kamel, "An efficient control strategy for enhancing frequency stability of multi-area power system considering high wind energy penetration," *IEEE Access*, vol. 8, pp. 140062–140078, 2020.

[5] G. Andersson, P. Donalek, R. Farmer, N. Hatziargyriou, I. Kamwa, P. Kundur, N. Martins, J. Paserba, P. Pourbeik, J. Sanchez-Gasca, R. Schulz, A. Stankovic, C. Taylor, and V. Vittal, "Causes of the 2003 major grid blackouts in north america and europe, and recommended means to improve system dynamic performance," *IEEE Trans. Power Syst.*, vol. 20, no. 4, pp. 1922–1928, Nov. 2005.

[6] R. Yan, N.-A.-Masood, T. K. Saha, F. Bai, and H. Gu, "The anatomy of the 2016 South Australia blackout: A catastrophic event in a high renewable network," *IEEE Trans. Power Syst.*, vol. 33, no. 5, pp. 5374–5388, Sep. 2018.

[7] M. Marzband, M. M. Moghaddam, M. F. Akorede, and G. Khomeyrani, "Adaptive load shedding scheme for frequency stability enhancement in microgrids," *Electr. Power Syst. Res.*, vol. 140, pp. 78–86, Nov. 2016.

[8] U. Rudez and R. Mihalic, "Predictive underfrequency load shedding scheme for islanded power systems with renewable generation," *Electr. Power Syst. Res.*, vol. 126, pp. 21–28, Sep. 2015.

[9] A. Rafinia, J. Moshtagh, and N. Rezaei, "Stochastic optimal robust design of a new multi-stage under-frequency load shedding system considering renewable energy sources," *Int. J. Electr. Power Energy Syst.*, vol. 118, Jun. 2020, Art. no. 105735.

[10] A. Rafinia, N. Rezaei, and J. Moshtagh, "Optimal design of an adaptive under-frequency load shedding scheme in smart grids considering operational uncertainties," *Int. J. Electr. Power Energy Syst.*, vol. 121, Oct. 2020, Art. no. 106137.

[11] N. Xia, H. B. Gooi, A. Abur, S. X. Chen, Y. S. F. Eddy, and W. Hu, "Enhanced state estimator incorporating adaptive underfrequency load shedding under contingencies via the alternating optimization method," *Int. J. Electr. Power Energy Syst.*, vol. 81, pp. 239–247, Oct. 2016.

[12] R. Horri and H. M. Roudsari, "Adaptive under-frequency load-shedding considering load dynamics and post corrective actions to prevent voltage instability," *Electr. Power Syst. Res.*, vol. 185, Aug. 2020, Art. no. 106366.

[13] T. Amraee, M. G. Darebaghi, A. Soroudi, and A. Keane, "Probabilistic under frequency load shedding considering RoCoF relays of distributed generators," *IEEE Trans. Power Syst.*, vol. 33, no. 4, pp. 3587–3598, Jul. 2018.

[14] S. Li, F. Tang, Y. Shao, and Q. Liao, "Adaptive under-frequency load shedding scheme in system integrated with high wind power penetration: Impacts and improvements," *Energies*, vol. 10, no. 9, p. 1331, Sep. 2017.

[15] K. Amarasekara, L. G. Meegahapola, A. P. Agalgaonkar, and S. Perera, "Characterisation of long-term voltage stability with variable-speed wind power generation," *IET Gener., Transmiss. Distrib.*, vol. 11, no. 7, pp. 1848–1855, May 2017.

[16] B. B. Adetokun, C. M. Muriithi, and J. O. Ojo, "Voltage stability assessment and enhancement of power grid with increasing wind energy penetration," *Int. J. Electr. Power Energy Syst.*, vol. 120, Sep. 2020, Art. no. 105988.

[17] J. Modarresi, E. Gholipour, and A. Khodabakhshian, "New adaptive and centralised under-voltage load shedding to prevent short-term voltage instability," *IET Gener., Transmiss. Distrib.*, vol. 12, no. 11, pp. 2530–2538, Jun. 2018.

[18] H. Bai and V. Ajjarapu, "A novel online load shedding strategy for mitigating fault-induced delayed voltage recovery," *IEEE Trans. Power Syst.*, vol. 26, no. 1, pp. 294–304, Feb. 2011.

[19] A. C. Adewole, R. Tzoneva, and A. Apostolov, "Adaptive under-voltage load shedding scheme for large interconnected smart grids based on wide area synchrophasor measurements," *IET Gener., Transmiss. Distrib.*, vol. 10, no. 8, pp. 1957–1968, May 2016.

[20] T. Shekari, A. Gholami, F. Aminifar, and M. Sanaye-Pasand, "An adaptive wide-area load shedding scheme incorporating power system real-time limitations," *IEEE Syst. J.*, vol. 12, no. 1, pp. 759–767, Mar. 2018.

[21] J. Tang, J. Liu, F. Ponci, and A. Monti, "Adaptive load shedding based on combined frequency and voltage stability assessment using synchrophasor measurements," *IEEE Trans. Power Syst.*, vol. 28, no. 2, pp. 2035–2047, May 2013.

[22] A. Wiszniewski, "New criteria of voltage stability margin for the purpose of load shedding," *IEEE Trans. Power Del.*, vol. 22, no. 3, pp. 1367–1371, Jul. 2007.

[23] J. A. Laghari, H. Mokhlis, M. Karimi, A. H. Abu Bakar, and H. Mohamad, "A new under-frequency load shedding technique based on combination of fixed and random priority of loads for smart grid applications," *IEEE Trans. Power Syst.*, vol. 30, no. 5, pp. 2507–2515, Sep. 2015.

[24] T. Shekari, F. Aminifar, and M. Sanaye-Pasand, "An analytical adaptive load shedding scheme against severe combinational disturbances," *IEEE Trans. Power Syst.*, vol. 31, no. 5, pp. 4135–4143, Sep. 2016.

[25] C. Li, Y. Wu, Y. Sun, H. Zhang, Y. Liu, Y. Liu, and V. Terzija, "Continuous under-frequency load shedding scheme for power system adaptive frequency control," *IEEE Trans. Power Syst.*, vol. 35, no. 2, pp. 950–961, Mar. 2020.

[26] H. Mortaji, S. H. Ow, M. Moghavvemi, and H. A. F. Almurib, "Load shedding and smart-direct load control using Internet of Things in smart grid demand response management," *IEEE Trans. Ind. Appl.*, vol. 53, no. 6, pp. 5155–5163, Nov. 2017.

[27] S. Manson, G. Zweigle, and V. Yedidi, "Case study: An adaptive under-frequency load-shedding system," *IEEE Trans. Ind. Appl.*, vol. 50, no. 3, pp. 1659–1667, May 2014.

[28] M. A. Kabir, A. H. Chowdhury, and N. Masood, "A dynamic-adaptive load shedding methodology to improve frequency resilience of power systems," *Int. J. Electr. Power Energy Syst.*, vol. 122, Nov. 2020, Art. no. 106169.

[29] T. Aziz, N.-A. Masood, S. R. Deeba, W. Tushar, and C. Yuen, "A methodology to prevent cascading contingencies using BESS in a renewable integrated microgrid," *Int. J. Electr. Power Energy Syst.*, vol. 110, pp. 737–746, Sep. 2019.

[30] P. Kundur, *Power System Stability and Control*. New York, NY, USA: McGraw-Hill, 1994, pp. 959–1022.

[31] C. Canizares, Ed., *Voltage Stability Assessment: Concepts, Practices and Tools*, Standard IEEE-PES Power System Stability SP101PSS, 2003.

[32] T. Green and C. Hamberg, *Pascal's Triangle*, 2nd ed. Scotts Valley, CA, USA: Createspace, 2012, pp. 65–140.

[33] T. Aziz, T. K. Saha, and N. Mithulananthan, "Identification of the weakest bus in a distribution system with load uncertainties using reactive power margin," in *Proc. 20th Australas. Universities Power Eng. Conf.*, Christchurch, New Zealand, 2010, pp. 1–6.
[34] M. Gibbard and D. Vowles, "Simplified 14-generator model of the SE Australian power system," Univ. Adelaide, Adelaide, SA, Australia, Tech. Rep. 3, Jun. 2010, vol. 3. [Online]. Available: http://www.eleceng.adelaide.edu.au/Groups/PCON/PowerSystems/IEEE/BenchmarkData/ Simplified_14-Gen_System_Rev3_20100701.pdf
[35] AEMO. (2019). *South Australian Electricity Report*. [Online]. Available: https://www.aemo.com.au/-/media/Files/Electricity/NEM/Planning_and_Forecasting/SA_Advisory/2019/2019-South-Australian-Electricity-Report.pdf
[36] AEMO. (2021). *Generation Information*. [Online]. Available: https://aemo.com.au/en/energy-systems/electricity/national-electricity-market-nem/nem-forecasting-and-planning/forecasting-and-planning-data/generation-information
[37] Australian PV Institute. (2021). *Solar PV Status*. [Online]. Available: https://pv-map.apvi.org.au/historical
[38] *PSS E—Power System Simulator for Engineering*, Siemens, Munich, Germany, 2021.

NAHID-AL-MASOOD (Senior Member, IEEE) received the B.Sc. and M.Sc. degrees in electrical and electronic engineering (EEE) from the Bangladesh University of Engineering and Technology (BUET), Dhaka, Bangladesh, in 2008 and 2010, respectively, and the Ph.D. degree in power and energy systems from the University of Queensland, Brisbane, Australia, in 2017. He is currently working as an Associate Professor with the Department of EEE, BUET. His research interests include power system modeling and analysis, and grid integration of renewable energy.

MD. NAHID HAQUE SHAZON (Student Member, IEEE) received the B.Sc. degree in electrical and electronic engineering (EEE) from the Bangladesh University of Engineering and Technology (BUET), Dhaka, Bangladesh, in 2019, where he is currently pursuing the M.Sc. degree in electrical and electronic engineering. He is currently working as a Lecturer with BRAC University, Dhaka. His research interests include power system analysis, grid integration of renewable energy, and solar cell research.

SHOHANA RAHMAN DEEBA (Member, IEEE) received the B.Sc. and M.Sc. degrees in electrical and electronic engineering (EEE) from the Bangladesh University of Engineering and Technology (BUET), Dhaka, Bangladesh, in 2009 and 2013, respectively, and the Ph.D. degree in power and energy systems from the University of Queensland, Brisbane, Australia, in 2017. She is currently working as an Assistant Professor with the Department of Electrical and Computer Engineering, North South University, Dhaka. Her research interests include encompass power system modeling, distribution system analysis, and renewable energy integration.

SEEMA RANI MODAK received the B.Sc. degree in electrical and electronic engineering (EEE) from Daffodil International University (DIU), Dhaka, Bangladesh, in 2018. Her research interests include power electronics and renewable energy.